

Numerical experiments on the intermediate asymptotics of shear-free turbulent transport and diffusion

By D. TORDELLA AND M. IOVIENO

Dipartimento di Ingegneria Aeronautica e Spaziale,
Politecnico di Torino, Corso Duca degli Abruzzi 24, 10129 Torino, Italy

(Received 3 May 2005 and in revised form 31 August 2005)

A numerical experiment on the interaction between different decaying homogeneous and isotropic turbulence is described. In the absence of kinetic energy production, the intermediate asymptotics of the turbulent shear-free mixing layer can be observed. The first aim of the experiment is to verify the existence of the intermittency or of the Gaussian asymptotic state in the case of the absence, or weak presence, of a lengthscale gradient. The second aim is to analyse the effects that are due to the difference between the spectral distribution of the interacting turbulence fields, which introduces the presence of the gradient of integral scale into the initial condition.

It can be observed that the homogeneity of the integral length across the shearless layer is not a sufficient condition to obtain the Gaussian asymptotic state. In fact, if the macroscale gradient is suppressed by considering turbulence with similar spectra, it is apparent that the intermittency increases with the energy gradient. Furthermore, by independently varying the initial energy level and distribution over the wavenumbers, two turbulence fields can be joined with an initial difference of integral scale either opposite to or concordant with the gradient of the turbulent kinetic energy. It is found that the intermittency and the depth of penetration by the eddies from the high-energy region increase when the energy and lengthscale gradients are concordant and decrease when they are opposite. Therefore, the most efficient process of mixing takes place when the spectra of two mixed fields differ in the lowest wavenumbers.

1. Introduction

The interaction of turbulence with different macroscales is common in nature and in engineering practice. In this context, shearless mixing is fundamental: this is the simplest inhomogeneous turbulent flow because it is free of turbulence production due to the presence of a mean shear. The macroscale gradient across the mixing layer is associated with the initial condition and the related spectral properties and is not necessarily oriented according to the energy gradient, as it can be concurrent or opposite to it.

A number of studies of the shearless mixing layer have been carried out to understand the interaction of two dominant energy-containing scales, see e.g. Gilbert (1980), Veeravalli & Warhaft (1989), Briggs *et al.* (1996), Knaepen, Debliquy, & Carati (2004). Veeravalli & Warhaft (in the following referred to as V&W) studied a turbulence mixing layer formed of decaying passive grid turbulences in which

two distinct scales interact. In this experiment, different kinds of grids and different lengthscale ratios were tested and the larger scale always belonged to the higher kinetic energy side of the stream. In all the tested cases, the mixing layer was very intermittent and the velocity statistics non-Gaussian. As a consequence, flow spreading was affected by both turbulent diffusion and intermittent turbulent penetration. The dependence on the initial conditions did not prevent self-similarity of the velocity statistical distributions from being reached with downstream distance. These results were in part different from Gilbert's (1980) observations, who did not find large-scale intermittency in his mixing layer. According to V&W, Gilbert's failure to observe intermittency was probably due to his experimental configuration, in which the energy ratio was equal to 1.48 and the mesh ratio was only 2, giving a lengthscale ratio of 1.4, which was considered too low a ratio to show a two-scale interaction process. In this interpretation, the mixing observed by Gilbert is an asymptotic state, where a transport process that is essentially controlled by a single scale, takes place: this results in a variance profile fitted by an error function, no intermittency, and thus global Gaussian behaviour (called turbulent diffusion).

The mixing layer simulation by Briggs *et al.* (1996) offers more information. This experiment has an initial energy ratio of about 7.5 and is initially a one-scale decaying mixing, since the initial condition presented an energy gradient that was produced by multiplying each spectral component in an initial homogeneous and isotropic velocity field by a factor which was only a function of the coordinate along the inhomogeneity direction x . This operation produces a profile of kinetic energy along x , but leaves the macroscale of the two initial turbulence fields thus built unaltered, according to the authors' integral scale definition (cf. Briggs *et al.* p. 218, formulae (2.9) and (2.10)). After a temporal evolution of 1.72 time units, and taking the Reynolds number effect into consideration, the unforced Briggs *et al.* simulation yields turbulence mixing with a macroscale ratio of nearly 0.93, a value that is closer to 1 than Gilbert's lengthscale ratio. It should be pointed out here that the Briggs *et al.* experimental simulation showed skewness and kurtosis distributions that were far from Gaussian, with intermittency data of the order of those of the 3:1 perforated plate experiment by V&W. This result is contrary to the existence of an asymptotic state when the macroscale gradient across the layer is weak (i.e. the lengthscale ratio is nearly one). In our opinion, the explanation of these findings lies in the very low energy gradient of Gilbert's mixing layer (1.48 as the energy ratio, against the value of 7.5 in the Briggs *et al.* experiment). In such a situation, it was very difficult for Gilbert to show the weak eventual removing of the velocity statistics from the Gaussian behaviour.

In this paper, we seek to verify this Gaussian asymptotic state by means of both direct and large-eddy numerical simulations (DNS and LES) where the gradient of kinetic energy is varied and the integral scale gradient is zero. In this case, a first kind of mixing, called type A, is obtained, which exchanges energy between turbulence with the same integral scale. We also carried out a numerical experimental analysis of the effects associated with a more general initial condition on the intermediate asymptotics (see Barenblatt 1996) of the turbulence mixing. In fact, the difference between the distributions of the kinetic energy on the wavenumbers of the two turbulence fields brings into play the presence of an integral scale gradient. By independently varying the intensity and the sign of the initial energy and integral scale gradients across the layer, a second and a third type of mixing are obtained, which exchange energy with an initial difference of integral scale either opposite to (type B) or concurrent with (type C) the gradient of the turbulent kinetic energy.

In this study, the adopted definition of the integral scale ℓ permits a direct measurement to be made and does not rely on the actual form of the link between the kinetic energy, the integral scale, the dissipation rate and the Reynolds number, which is far from being accurately known (see Batchelor 1953; Sreenivasan 1998; Kaneda *et al.* 2003). Details concerning the statistical definitions, filtering techniques and numerical simulations are given in §2. Section 3 contains a description of the results obtained using the DNS and LES of the three kinds of mixing layer. The main findings are summarized in the conclusions (§4).

2. Determination of turbulence macroscales, filtering and numerical details of the simulations

The definition of a longitudinal integral scale that permits a direct measurement is

$$\ell(t) = \frac{1}{3} \sum_i \frac{\int_0^\infty R_{ii}(r, t) \, dr}{R_{ii}(0, t)}, \quad (2.1)$$

where R_{ii} is the longitudinal velocity correlation (see e.g. Batchelor 1953, p. 105). Since ℓ is a quantity normalized by the kinetic energy, the integral scale does not depend on the level of the kinetic energy, but on the way it is distributed over the wavenumbers (in particular over the small wavenumbers which are not universal in behaviour since they depend on the geometry of the boundaries). It is thus possible, depending on the initial/boundary conditions, that a flow region which is rich in kinetic energy has a lower macroscale than an adjacent region which is poorer in energy. It is also evident that turbulence with a similar spectrum has equal macroscale, regardless of the energy content. It is therefore possible to have initial conditions where a zero macroscale gradient is associated with the presence of an energy gradient.

In literature dealing with shearless mixing, authors often use approximations of the integral length deduced from the hypothesis of statistical equilibrium, i.e.

$$\ell = \frac{E^{3/2}}{\epsilon}, \quad (2.2)$$

where $dE/dt = -\epsilon$. However, in the Briggs *et al.* (1996) and Knaepen *et al.* (2004) DNS simulations, in the laboratory experiments by V&W, as well as in the present DNS simulations, this hypothesis is not fully satisfied, since the Taylor-microscale Reynolds numbers (Re_λ) are less than 70, see Batchelor (1953), Dimotakis (2000). Relation (2.2) should be applied with caution whenever the Re value does not allow the divergence of scales to be obtained that the universal equilibrium theory requires. At low Reynolds numbers, (2.2) should be replaced by

$$\frac{\ell\epsilon}{E^{3/2}} = f(Re). \quad (2.3)$$

Function f is of order 1, but is not yet completely known. Simulations of homogeneous and isotropic turbulence in a periodic box and the laboratory, see Batchelor (1953), Sreenivasan (1998), Kaneda *et al.* (2003), show that, in the low Re range, its value almost halves when Re quadruples. As a consequence, and recalling that during decay Re_λ remains constant (Speziale 1992), an integral length ratio estimated with relation (2.2) can be affected by a large error. In the following, we use definition (2.1), which is equivalent to (2.3). We have also listed the integral scale

	$\mathcal{E} = \frac{E_1}{E_2}$	$\nabla_*(E/E_1)$	$\mathcal{L} = \frac{\ell_1}{\ell_2}$	$\nabla_*(\ell/\ell_1)$	Re_{λ_1}	n_1	n_2	$\frac{x_s - x_c}{\Delta}$	$\frac{x_k - x_c}{\Delta}$
DNS: A	6.7	0.425	1.0 (1.6)	0.0	45.4	1.22	1.16	0.42	0.62
B	6.6	0.424	0.6 (0.5)	-0.33	45.4	1.22	1.32	0.36	0.45
C1-s	6.6	0.424	1.5 (1.7)	0.17	45.4	1.22	1.39	0.63	0.84
C1-c	6.5	0.423	1.5 (1.8)	0.17	45.4	1.22	1.37	0.63	0.84
C2	6.5	0.423	2.1 (2.7)	0.26	45.4	1.22	1.56	0.79	0.98
LES: a1	1.43	0.149	1.0	0.0	45	1.25	1.16	0.17	0.30
a2	6.7	0.421	1.0	0.0	45	1.25	1.15	0.54	0.75
a3	12.1	0.454	1.0	0.0	45	1.23	1.15	0.65	0.86
	12.1	0.454	1.0	0.0	450	1.20	1.14	0.72	0.93
a4	24.0	0.474	1.0	0.0	45	1.22	1.13	0.82	0.99
	24.0	0.474	1.0	0.0	450	1.20	1.13	0.86	1.06
a5	58.1	0.485	1.0	0.0	45	1.22	1.13	1.07	1.23
	58.1	0.485	1.0	0.0	450	1.20	1.13	1.19	1.28
b1	24.0	0.474	0.53	-0.44	45	1.24	1.35	0.72	0.86
b2	58.0	0.485	0.38	-0.80	45	1.20	1.11	0.80	0.91
V&W – bars	6.2		(2.4)		78.1	1.22	1.39	0.30	0.30
V&W – plate	6.3		(2.2)		44.5	1.43	1.25	0.63	0.81
Briggs <i>et al.</i>	7.5		1.0(1.7)		40.3	1.55	1.35	0.38	0.51
Knaepen <i>et al.</i>	6.27		(2.2)		69.0	1.30	1.10	0.77	1.06

TABLE 1. Flow parameters. E = kinetic energy, ℓ = integral scale (equation (2.1)), Re_{λ} = Taylor-microscale Reynolds number, $\nabla_* = \partial/\partial(x/\Delta)$ = gradient normalized with the mixing layer thickness Δ , n = exponent of the energy decay, x_s and x_k are the positions of the maxima of skewness and kurtosis. Index 1 refers to the high-energy region, index 2 to the low-energy region. In the fourth column, the data in parenthesis refer to scales computed through equation (2.2).

ratio estimated using (2.2) in table 1 for all our simulations to show the size of the approximation induced by the adoption of the hypothesis of statistical equilibrium.

To produce different turbulence scales, it is possible to filter the available original turbulent field (Wray 1998) to obtain a new field with a different spectral distribution of energy. To form the initial condition, the original and the new field are placed side-by-side in the computational domain using the technique by Briggs *et al.* (1996), which matches the turbulence through a rapid transition layer. The low-pass filtering of the fluctuation field leads to an increase of the integral scale, while the high-pass filtering leads to a decrease. When two turbulence fields are obtained by multiplying the same initial velocity field by a constant, the numerical experiment carried out by mixing these fields is initially an example of turbulence mixing with different energies but equal integral scales. If the fundamental definition of a longitudinal integral scale is applied, see (2.1), the ratio of the integral scales of the turbulences will be equal to 1.

In this study, one low-pass and two high-pass filtering methods were adopted. The low-pass filtering has been obtained through the direct numerical simulation of the decay of the homogeneous isotropic field used to prepare the initial conditions (Wray 1998). A decayed field has low energy and a larger scale than the initial field. Thus, the numerical mixing of the decayed and the initial fields permits a shearless layer to be obtained with opposite energy and integral scale gradients. The following filters were used to high-pass filter the turbulence fluctuations:

$$g_s(\mathbf{k}) = \frac{1}{1 - e^{-a(|\mathbf{k}| - |\mathbf{k}_0|)}}, \quad (2.4)$$

$$g_c(\mathbf{k}) = \prod_i \phi(k_i), \quad \phi(k_i) = \frac{1}{1 - e^{-a(k_i - k_0)}}. \quad (2.5)$$

Function g_s is a spherical kind of filter. Function g_c filters any wavenumber that has at least one component lower than the filter scale, k_0 , and thus suppresses the filamented and layered structures from the turbulence. This second kind of filter, which can be called cross-filtering, is more efficient in lowering the integral scale of the turbulence than the spherical one and is thus used to produce the mixing with the highest lengthscale ratio. The same mixing was produced using both the spherical and the cross-filters to check for the existence of initial condition effects that can be attributed to the filtering used and non-exclusively to the global statistical properties of the initial condition. The statistics in the self-similar part of the decay were then compared, but no significant difference was observed (see § 3, and figure 1*b*). It should be noted that after the filtering and before the initialization of the field, the turbulence was always time evolved to obtain a Navier–Stokes field.

The initial condition can be prepared in an alternative manner. Knaepen *et al.* (2004) initialized the flow by using Fourier modes associated with the velocity field, fixing their amplitude to match a given spectrum and assigning them random phases. The procedure starts from the initialization of three-dimensional modes, that are then transformed into two-dimensional Fourier modes, rescaled on the prescribed two-dimensional spectra in each plane perpendicular to the direction of inhomogeneity, and then transformed back into three-dimensional modes. The procedure also includes iterations with projection onto divergence-free fields to satisfy continuity, and time evolving the flow to obtain a Navier–Stokes solution from the random phases. However, procedures based on the random-noise turbulence generation methods are generally rather slow in establishing realistic turbulence compared to recycling methods based on the use of data from a separate calculation (see e.g. Keating *et al.* 2004). For this reason, to reduce the turbulence integral scale, we preferred to use the simpler method based on the high-pass filtering of an original Navier–Stokes solution followed by a development run which exploits a temporal evolution (lasting approximately one eddy turnover time) to restore the properties relevant to the Navier–Stokes fields.

The direct numerical simulations presented here were carried out by means of a new technique for the parallel dealised pseudospectral integration of the Navier–Stokes equations (Iovieno, Cavazzoni, & Tordella 2001). The boundary conditions are periodic in all directions. Two computational domains, a $(2\pi)^3$ cube with 128^3 points, and a $4\pi(2\pi)^2$ parallelepiped with 256×128^2 points, were used to obtain an estimate of the numerical accuracy. In the initial condition, the two velocity fields are matched by means of a hyperbolic tangent function, which has width $1/20$ of the domain (but $1/40$ for the larger domain):

$$\mathbf{u}(\mathbf{x}) = \mathbf{u}_1(\mathbf{x})p(x) + (1 - p(x))\mathbf{u}_2(\mathbf{x}),$$

$$p(x) = \frac{1}{2} \left[1 + \tanh \left(a \frac{x}{L} \right) \tanh \left(a \frac{x - L/2}{L} \right) \tanh \left(a \frac{x - L}{L} \right) \right],$$

where x is the inhomogeneous direction, L is the width of the computational domain and constant $a = 12\pi$, see figure 1(*a*). This technique of generation of the transition layer is analogous to that used in Briggs *et al.* (1996) and Knaepen *et al.* (2004). The time integration is carried out by means of a four-stage fourth-order explicit Runge–Kutta scheme. The same numerical technique was used to implement the

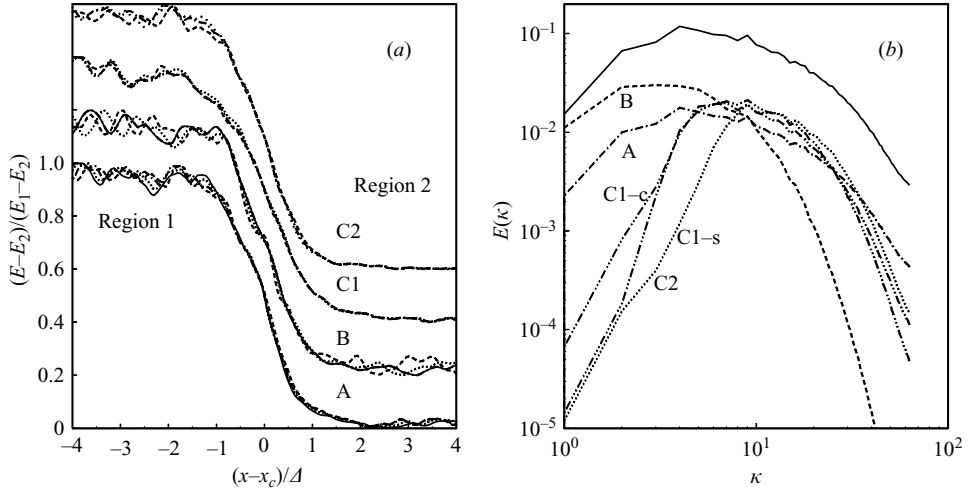


FIGURE 1. (a) Normalized kinetic energy: x_c is the mixing layer centre and Δ is the mixing layer thickness. (b) Initial three-dimensional energy spectra. Continuous line: high-energy region for all the mixing types; other lines: low-energy region for mixing A, B, C1-c, C1-s and C2.

large-eddy simulations, which were carried out using the Intrinsic Angular Momentum (IAM) subgrid-scale model (Iovieno & Tordella 2002). This model is based on the proportionality of the turbulent diffusivity to the intrinsic moment of momentum of the finite element of a fluid. The IAM correctly scales the eddy diffusivity ν_δ , with respect to both the filtering length and the dissipation rate, and introduces a differential equation – the intrinsic angular momentum equation – to follow the evolution of ν_δ . This is particularly advantageous in the case of non-equilibrium turbulence fields, since it adds a degree of freedom to the subgrid modelling.

This section is concluded with information on accuracy estimates deduced *a posteriori*. The source of all the turbulence fields used was the direct numerical simulation of homogeneous and isotropic turbulence by Wray (1998). The raw data by Wray presented an inhomogeneity level for the kinetic energy of about $\pm 8\%$ and skewness and kurtosis values slightly different from those of the statistical equilibrium (respectively 0.02 ± 0.2 instead of 0 and 2.8 ± 0.3 instead of 3). For our set of direct numerical simulations, the widening of the computational domain from 2π to 4π (from 128 to 256 grid points) along the inhomogeneous direction, gave estimates of the relative accuracy of about 5% for the maximum values of the distributions of the skewness, and of about 12% for the kurtosis distributions, and it increased the signal-to-noise ratio from 4.5 to 7 for the skewness computation, and from 4 to 5 for the kurtosis computation. The large-eddy simulations were performed over 64^3 grid points. It has been verified, by means of tests with an enhanced spatial discretization (32^3 , 48^3 and 64^3 grid points), that, for the observed temporal evolution, the two equilibrium turbulence fields outside the mixing region have a non-homogeneity of about $\pm 5\%$. For the skewness and kurtosis distributions, the signal-to-noise ratio is lower than that of the DNS, and it is equal to about 4 and 3 , respectively.

3. Simulation results and discussion

The initial conditions place a kinetic energy and an integral scale gradient in the direction of inhomogeneity (here denoted x). The gradients result from the different

levels of kinetic energy of the two interacting turbulence fields, each of which can be characterized by a different macroscale. In the following the indexes 1 and 2 indicate the high- and the low-energy fields, respectively, see figure 1(a). The parameters that are actually controlled in the experiment are the ratio of energy, $\mathcal{E} = E_1/E_2$, which is taken to be greater than 1 in all the simulations, and the ratio of integral scales, $\mathcal{L} = \ell_1/\ell_2$, which can be either greater than 1 (concurrent energy and scale gradients), equal to 1 (zero scale gradient) or lower than 1 (opposite gradients). The centre x_c of the mixing layer is the position where $E = (E_1 + E_2)/2$.

The flow parameters of the present simulations are documented in table 1, together with the parameters of the experiments by V&W and the simulations by Briggs *et al.* (1996) and Knaepen *et al.* (2004). The values of the normalized gradients relevant to the imposed energy and scale ratios are also given in table 1. In the gradients, the energy and integral scale are normalized by the values of the high energy field, while the spatial coordinate is normalized by the length $\Delta(t)$. Function Δ is defined by mapping the low-energy side of the mixing layer to zero and the high-energy side to one, and it is equal to the distance between the points with energy values 0.25 and 0.75, as in the paper by V&W. It should be noticed that by doing so, the energy gradient value has the upper limit of 0.5, which is reached in the limit for E_2 going to zero, i.e. when $E_2/E_1 \rightarrow 0$ ($\mathcal{E} \rightarrow \infty$).

Outside the mixing region, the kinetic energy in the two turbulence fields decays as

$$E = A(t + t_0)^{-n} \tag{3.1}$$

(Batchelor 1953). Here, t and t_0 are the non-dimensional time and decay constants of integration, respectively, which are normalized by the field eddy turnover time $\tau = \ell/E^{1/2}$. Constant A is equal to $E(0)t_0^n$. The dissipation rate is $\epsilon = -dE/dt$. Relation (2.3) yields the following the temporal variation for the macroscale:

$$\ell = \frac{1}{n} f(Re_\lambda) \sqrt{A} (t + t_0)^{1-n/2}. \tag{3.2}$$

As a consequence, since the values of the exponents n_1, n_2 and of the constants t_{01}, t_{02} are close to each other, see table 1, functions

$$\frac{\mathcal{L}(t)}{\mathcal{L}(0)} = \left(1 + \frac{t}{t_{01}}\right)^{1-n_1/2} \left(1 + \frac{t}{t_{02}}\right)^{-1+n_2/2}, \tag{3.3}$$

$$\frac{\mathcal{E}(t)}{\mathcal{E}(0)} = \left(1 + \frac{t}{t_{02}}\right)^{n_2} \left(1 + \frac{t}{t_{01}}\right)^{-n_1} \tag{3.4}$$

slowly vary in time. This permits the mixing evolution to take place under nearly constant conditions.

Independently of the values of the control parameters and the concurrency, or lack of it, of the energy and scale gradients, a set of common properties exists for all the studied mixing. First, the statistical distributions become self-similar after a decay of nearly three time units. Second, in the self-similarity region of the decay, the lateral spreading rate is on average close to 0.15. Third, the kinetic energy distribution has a common shape, as can be seen in figure 1(a). Fourth, all the mixing layers – including the mixing with $\mathcal{L} = 1$, case A – are very intermittent, as the skewness S and kurtosis K distributions show, see figures 2–5.

The experiment by Gilbert (1980), where $\mathcal{L} = 1.4$ and $\mathcal{E} = 1.48$ and the turbulent transport was observed to be diffusive, could be interpreted as a one-scale mixing

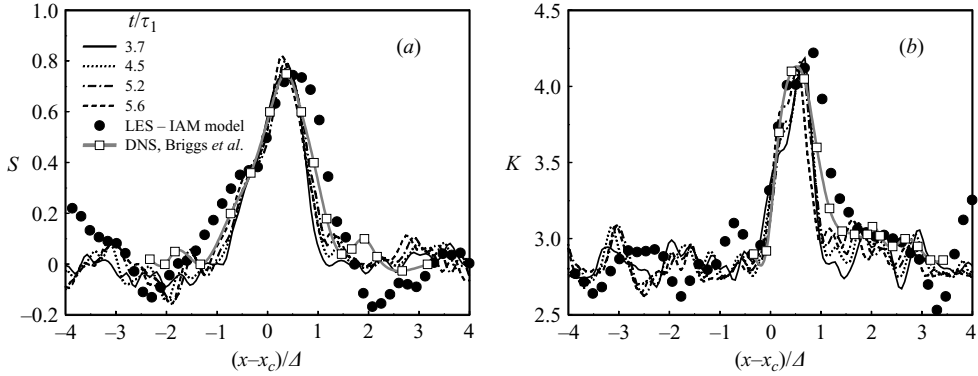


FIGURE 2. Skewness (a) and kurtosis (b) of the velocity component in the inhomogeneous direction x for case A ($\mathcal{E} = 6.7$, $\mathcal{L} = 1.0$): x_c is the mixing layer centre, Δ the mixing layer thickness and $\tau_1 = \ell(0)/E_1(0)^{1/2}$. Data from Briggs *et al.* (1996) and Iovieno & Tordella (2002) are also shown.

layer, i.e. nominally mixing with $\mathcal{L} = 1$. Then, the Gaussianity of the transport could be hypothesized as a feature of the *asymptotic state* of the shearless mixing, which is the state that is supposedly encountered when the lengthscale ratio is close to one and the production of kinetic energy due to the mean flow and fluctuation interaction is absent. In this situation, the mixing is viewed as a region of large variance diffusing into a region of lower variance. We have studied this problem by carrying out a series of numerical simulations with $\mathcal{L} = 1$ and an increasing value of \mathcal{E} , that are here called experiments of kind A. Numerically, mixing A can be produced by letting two turbulence fields with different energies but a similar spectrum shape interact, see figure 1(b) and the preceding paragraph. In the DNS for A, mixing with $\mathcal{L} = 1$ is coupled to an energy gradient $\nabla_* E = -0.42$ ($\mathcal{E} = 6.7$, that is, the energy ratio studied by V&W). A large intermittency has been observed in this simulation, see figure 2.

It should be recalled that the numerical experiment on unforced mixing by Briggs *et al.* (1996) is also of this kind (see § 1 above and § 2.1, formula 2.2 Briggs, *et al.*). In fact, their lengthscale ratio remained very close to one, as is possible to verify after having deduced the value of constant $t_{01} = 0.5$ from the decay of their high-energy homogeneous region (cf. figure 3, Briggs *et al.*), and of constant $t_{02} = 0.68$ (from table 1, Briggs *et al.* and from (3.1), (3.2)). The constant t_{02} has been also deduced by noting that, due to the technique used, in the initial condition the high- and the low-energy regions have similar spectra at $t = 0$, and thus have the same integral scale, $\mathcal{L}(0) = 1$ (see also figure 2, Briggs *et al.*). At $t = 1.72$ time units, the unforced Briggs *et al.* (1996) mixing shows $\mathcal{L} = 0.93$, and skewness and kurtosis maxima of 0.75 and 4.2, respectively. These values are very close to the present simulation, see figure 2.

The present simulation, A, and the Briggs *et al.* (1996) results do not confirm the asymptotic hypothesis. In figure 2, the results from LES obtained using the IAM subgrid-scale model (Iovieno & Tordella 2002) are also shown. By means of LES, which allow a reduction of 20 times the computational time, the energy gradient in experiment A was increased from zero, $\mathcal{E} = 1$, to about 0.5, $\mathcal{E} = 58$, see figure 6(a, b) below. A regular increase in intermittency characteristics, such as the position of the maxima in the skewness x_s and kurtosis x_k distribution, with the energy gradient was observed. These positions x_s and x_k represent the penetration of the turbulence mixing,

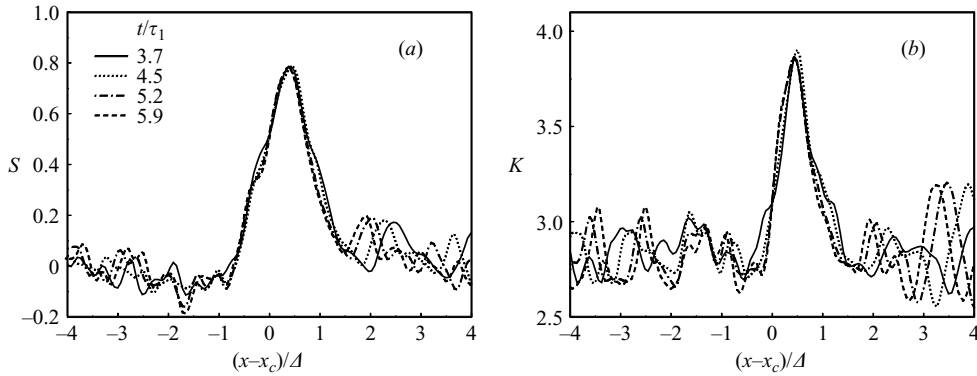


FIGURE 3. (a) Skewness and (b) kurtosis for case B ($\mathcal{E} = 6.6$, $\mathcal{L} = 0.6$). Details as in figure 2.

that is, the planes across which the flow of the second moment of the momentum fluctuations – the turbulence kinetic energy – and the third moment is maximized. This increase, in particular the arithmetic mean of x_s and x_k , if viewed as a function of \mathcal{E} , corresponds to a map with a scaling exponent of about 0.29

$$\frac{\eta_s + \eta_k}{2} \sim a \left(\frac{E_1}{E_2} - 1 \right)^b, \quad a \simeq 0.36, \quad b \simeq 0.298, \tag{3.5}$$

where $\eta = (x - x_c)/\Delta$, see figure 6(a). If the intermittency increase is viewed as a function of the normalized energy gradient, observing that approximately $\nabla_*(E/E_1) \simeq (1 - \mathcal{E}^{-1})/2$, the scaling is

$$\frac{\eta_s + \eta_k}{2} \sim a \left(\frac{2\nabla_*(E/E_1)}{1 - 2\nabla_*(E/E_1)} \right)^b, \tag{3.6}$$

see figure 6(b). This result, as well as the previous ones, have been obtained at the Reynolds number based on the Taylor microscale of 45, which is the value most often considered in the shear-free mixing literature. To check for the existence of major Reynolds number effects, capable of spoiling the quality of the results produced by these numerical experiments, we have repeated a few LES of kind A at a Reynolds number ten times larger, i.e. 450. Figure 6(b) below includes these simulations and shows that the agreement between the simulations carried out at $Re_\lambda = 45$ and at 450 is good.

To improve and complete the experimental analysis of this mixing process, we decided to change the value $\mathcal{L} = 1$ by carrying out direct numerical simulations, as well as LES, with $\mathcal{L} < 1$ (opposite energy and lengthscale gradients), case B, and with $\mathcal{L} > 1$ (concordant energy and lengthscale gradients), case C.

Case B, documented in figure 3 (a, b) and table 1, has been obtained by matching a high-energy turbulence and a low-energy turbulence, obtained through the decay of field 1 over 2.4 time scales. The decayed turbulence has a larger scale, therefore the energy and integral scale gradients are opposite. In this case, a decrease in the intermittency can be observed since both the maxima of functions S , K and the lateral penetration are lowered with respect to case A, see figure 6. It should be noted that, in figure 6(a), all the mixing of type B falls below the map that describes the mixing of type A.

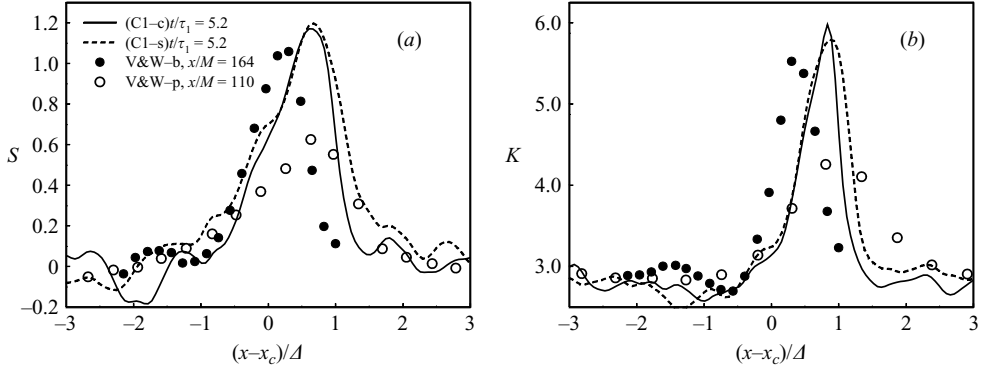


FIGURE 4. (a) Skewness and (b) kurtosis for case C1 ($\mathcal{E} = 6.3$, $\mathcal{L} = 1.5$). Details as in figure 2. Symbols: experimental data from V&W (1989), see table 1.

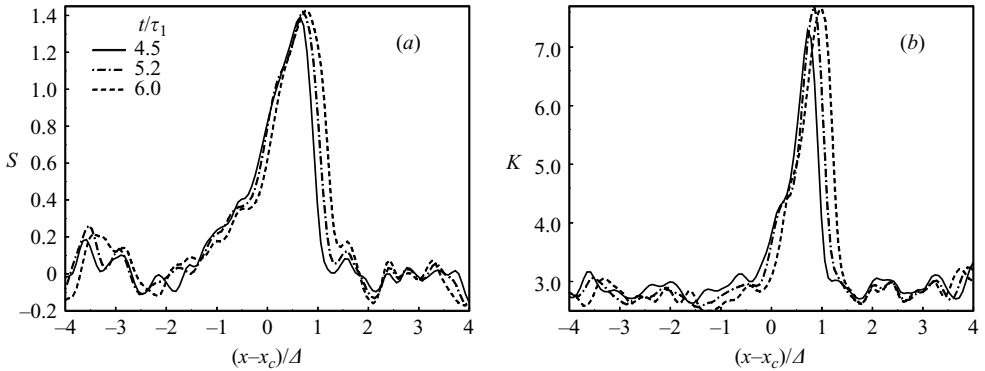


FIGURE 5. (a) Skewness and (b) kurtosis for case C2 ($\mathcal{E} = 6.2$, $\mathcal{L} = 2.1$). Details as in figure 2.

Case C is described in figures 4 (mixing C1) and 5 (mixing C2). Simulation C1 reproduces a flow configuration that is similar to the experiments of the 3.3:1 parallel bars and the 3:1 perforated plate by V&W, two experimental versions of mixing with a lengthscale ratio close to 2 (but close to 1.5, if the Reynolds number effect is accounted for, see §2 and table 1). This configuration is characterized by the concurrency of the energy and scale gradients. The agreement between our simulation and the V&W data is good, see figure 4. It can be observed that the intermittency is enhanced with respect to case A, see also figure 6. The simulation falls somewhere between the two V&W experiments, though it is closer to the 3.3:1 parallel bar data, which is a good sign, given that V&W trusted the parallel bar more than the perforated plate data. It should be noted that we have included data, in figure 4, from two simulations (C1-s, C1-c) carried out by the high-pass filtering region 2 with filters (2.4) and (2.5). These two simulations basically yield the same results and this permits us to use the cross-filter with confidence to increase \mathcal{L} to the value 2.1 (table 1, mixing C2 data, see also figure 5 for this mixing). In this case, the intermittency is further increased, see figure 7, with respect to experiment A and, as a consequence, also with respect to experiment B. This confirms that the turbulent transport is more efficient when the

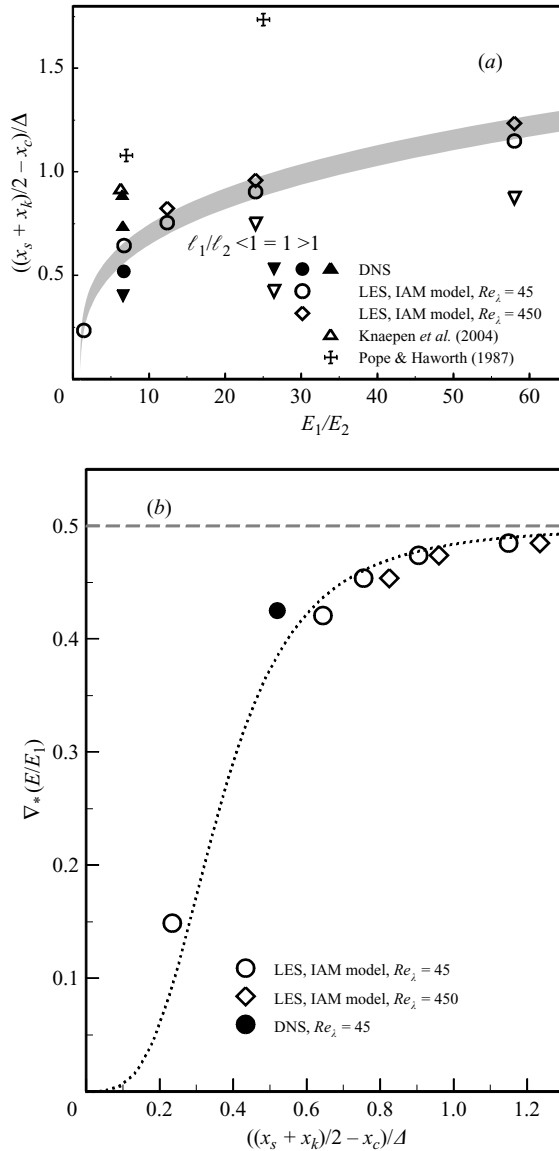


FIGURE 6. Positions, x_s and x_k , of the maxima of the skewness and kurtosis distributions. (a) As a function of the initial ratio of energy in experiments A,B and C. The grey region represents equation (3.5) with an uncertainty level of ± 0.05 . (b) As a function of the initial gradient of energy in experiment A. The dotted line corresponds to equation (3.6). The dashed line represents the limit value of the normalized energy gradient.

local integral scale gradient has the same sign as the energy gradient. It should be noted in figure 6(a) that the mixing with $\mathcal{L} > 1$, including the model computations by Pope & Haworth (1995), fall above the map that represents the mixing with $\mathcal{L} = 1$. According to these results, the one-scale shearless turbulence mixing cannot be considered an asymptotic state. In fact, the transport properties vary continuously across the zero gradient of the integral scale.

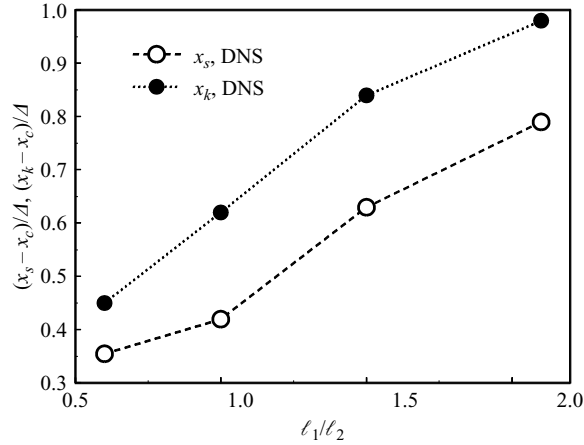


FIGURE 7. Position of the maximum of the skewness and kurtosis distributions as a function of the initial ratio of integral scale: x_s and x_k are the positions of the maximum of $S(x)$ and $K(x)$, respectively.

4. Conclusions

The intermediate asymptotics of turbulent mixing layers in the absence of the production of turbulent kinetic energy has been considered. This requires analysing the dependence on the initial condition, which here has been documented through single-point statistics. Three kinds of shearless turbulence mixing were studied, a first kind with a zero macroscale gradient, and a second and a third kind with opposite and concordant energy and scale gradients, respectively. In all cases, a self-similar state appears to exist which is reached after a decay of nearly 3 time units. The statistical distributions of orders higher than the second maintain features that depend on the initial values of the kinetic energy, \mathcal{E} , and macroscale, \mathcal{L} , ratios, and on the sign of $\Delta\mathcal{L}$.

If the energy ratio is far from unity, no Gaussian behaviour is observed up to moments of the order of four for mixing with $\mathcal{L} \approx 1$. The asymptotic state for the shearless turbulence, where the velocity variance follows the form of an error function and the velocity fluctuations are Gaussian, was not observed. On the contrary, the mixing is very intermittent and the intermittency characteristics vary smoothly when passing through $\mathcal{L} = 1$. If the lateral penetration is considered in terms of the position of the maxima of skewness and kurtosis distributions, it is possible to deduce, that, when $\mathcal{L} = 1$, the intermittency increases with the energy ratio with a scaling exponent that is approximately equal to 0.29. The relevant map splits the plane $\{\text{penetration}, \mathcal{E}\}$ into two regions: a region where the penetration is lower and where all the mixing mapped there is observed to have $\mathcal{L} < 1$, which in turn means opposite lengthscale and energy gradients; and a region where the penetration is higher and where all the mapped mixing is found to have $\mathcal{L} > 1$, meaning concurrent lengthscale and energy gradients. This implies that mixing with $\mathcal{L} = 1$ does not represent an asymptotic state of no, or low, intermittency and that, to obtain mixing that behaves as a region of large variance diffusing in a region of lower variance, it is also necessary for the energy ratio to be close to one.

If the energy ratio is kept constant, the maximum values of both the skewness and the kurtosis increase with the lengthscale ratio. Higher values than when $\mathcal{L} = 1$ are observed if the energy and scale ratios are concordant, and lower values if opposite.

From this it is possible to deduce that the sign of the integral scale gradient controls the turbulence mixing process. When $\nabla E \cdot \nabla \ell > 1$ the flow and variance of the turbulent kinetic energy are more intense and the transport process is maximized in planes that are more laterally displaced with respect to the centre of the initial mixing than when $\nabla E \cdot \nabla \ell < 1$.

REFERENCES

- BARENBLATT, G. I. 1996 *Scaling, Self-similarity, and Intermediate Asymptotics*, Preface, p. xiii Cambridge University Press.
- BATCHELOR, G. K. 1953 *The Theory of Homogeneous Turbulence*. Cambridge University Press.
- BRIGGS, D. A., FERZIGER, J. H., KOSEFF, J. R. & MONISMITH, S. G. 1996 Entrainment in a shear-free turbulent mixing layer. *J. Fluid Mech.* **310**, 215–241.
- DIMOTAKIS, P. E. 2000 The mixing transition in turbulent flows. *J. Fluid Mech.* **409**, 69–98.
- GILBERT, B. 1980 Diffusion mixing in grid turbulence without mean shear. *J. Fluid Mech.* **100**, 349–365.
- KANEDA, Y., TAKASHI, I., YOKOKAWA, M., ITAKURA, K. & UNO, K. 2003 Energy dissipation rate and energy spectrum in high resolution direct numerical simulations of turbulence in a periodic box. *Phys. Fluids* **15**, L21–24.
- KEATING, A., PIOMELLI, U., BALARAS, E. & KALTENBACH, H. J. 2004 A priori and a posteriori test of inflow conditions for large-eddy simulation. *Phys. Fluids* **16**, 4696–4712.
- KNAEPEN, B., DEBLIQUY, O. & CARATI, D. 2004 Direct numerical simulation and large-eddy simulation of a shear-free mixing layer. *J. Fluid Mech.* **414**, 153–172.
- IOVIENO, M., CAVAZZONI, C. & TORDELLA, D. 2001 A new technique for a parallel dealiased pseudospectral Navier-Stokes code. *Comput. Phys. Commun.* **141**, 365–374.
- IOVIENO, M. & TORDELLA, D. 2002 The angular momentum for a finite element of a fluid: A new representation and application to turbulent modeling. *Phys. Fluids* **14**, 2673–2682.
- POPE, S. B. & HAWORTH, D. C. 1987 The mixing layer between turbulent fields of different scales. In *Turbulent Shear Flows 5* (ed. L. T. S. Bradbury *et al.*), pp. 44–53. Springer.
- SPEZIALE, C. G. 1992 The energy decay in self-preserving isotropic turbulence revisited. *J. Fluid Mech.* **241**, 645–667.
- SREENIVASAN, K. R. 1998 An update on the energy dissipation rate in isotropic turbulence. *Phys. Fluids* **10**, 528–529.
- VEERAVALLI, S. & WARHAFT, Z. 1989 The shearless turbulence mixing layer. *J. Fluid Mech.* **207**, 191–229 (referred to herein as V&W).
- WRAY, A. A. 1998 Decaying Isotropic Turbulence. In *A Selection of Test Cases for the Validation of Large-Eddy Simulations of Turbulent Flows*, HOM02, pp. 63–64. AGARD-AR-345.